Available on CMS information server CMS CR 2003/027

CMS Conference Report

Physics reach with CMS at high and super-high luminosities

James W. Rohlf
Boston University, Boston MA, 02215 USA
e-mail: rohlf@bu.edu

EPJdirect A1, 1–11 (2003)
DOI 10.1007/s1010503a123

EPJdirect
electronic only

Physics reach with CMS at high and super-high luminosities

James W. Rohlf

Boston University, Boston MA, 02215 USA
e-mail: rohlf@bu.edu

Received:

Abstract. The physics reach of the Compact Muon Solenoid, under construction to study proton-proton collisions at a centre-of-mass energy of 14 TeV, is presented at design luminosity of $10^{34}\mathrm{cm}^{-2}\mathrm{s}^{-1}$ and beyond ($10^{35}\mathrm{cm}^{-2}\mathrm{s}^{-1}$). The sensitivity for detection of the standard-model Higgs boson in the channels qqH (W fusion), WH, and tH is discussed with the result that the Higgs boson is observable in multiple decay modes over entire mass range, 0.1-1 TeV/c^2. Higgs boson searches for decays involving taus in the context of the Minimal Supersymmetric Standard Model result in a limit of about 0.6 TeV/c^2 at tanβ=25. Sparticle reconstruction for decays containing leptons and jets results in a squark/gluino mass reach in the range 2.5-3 TeV/c^2. Limits on Kaluza-Klein excitations of the graviton or a new heavy vector boson are in the 5-6 TeV/c^2 range. The scattering of vector bosons at high energy and discovery potential for compositeness is described.

PACS: 11.30.Pb; 12.38.Qk; 12.60.Fr; 12.60.Fr; 12.60.Jv; 12.60.Rc; 14.60.Cd; 14.60.Ef; 14.60.Fg; 14.65.Fy; 14.65.Ha; 14.80.Bn; 14.80.Cp; 14.80.Ly; 14.70.Fm; 14.70.Hp; 14.70.Pw

1 Introduction

The standard model (SM) of particle physics has been constructed brick-by-brick over the last few decades by incorporating all available experimental information into one consistent, albeit incomplete, description of electroweak and strong interactions. The major milestones include the discoveries of charm, the third lepton family, and the third quark family, the observation of neutral currents and the W and Z bosons, determination of three light neutrinos and many other detailed measurements from LEP, as well as the experimental tests of quantum chromodynamics (QCD) at high energy. There remains but one necessary particle, the Higgs boson, to be discovered in order to complete our understanding of nature at energy scales below a few hundred GeV. It is implausible, however, to expect today's SM to work at energy scales all the way to the Planck mass.

In the big picture (Fig 1), LHC physics may be viewed as the first look at the TeV/c^2 mass scale to find a clue to the solution to the hierarchy problem... *what lies between the electroweak scale and the Planck mass?* In a somewhat more limited view, the LHC will explore the mechanism for electroweak symmetry breaking... *How do the W and Z^0 interact at high energies?* In a yet narrower

view, but important nevertheless, the LHC will serve to nail down the elusive Higgs particle.

Big Picture

FIRST look at the TeV/c^2 mass scale to find a clue to the hierarchy problem... *What lies between the weak scale and the Planck mass?*

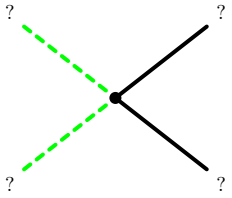

Medium Picture

EXPLORE the mechanism for electroweak symmetry breaking... *How do the W/Z^0 interact at high energies?*

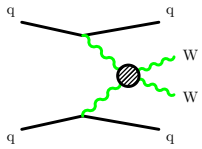

Small Picture

NAIL down the elusive Higgs boson...

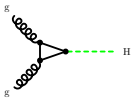

Fig. 1. The LHC *raison d'être.*

1.1 Rates

The Compact Muon Solenoid (CMS) detector [1], shown in Figs. 2-3, is designed to explore the physics accessible with the Large Hadron Collider (LHC) presently under construction at CERN. The machine is designed to collide protons at a centre-of-mass energy of 14 TeV and a luminosity of 10^{34} cm^{-2}s^{-1}, referred to as "high" luminosity [2]. An upgrade to the LHC [3] could bring the luminosity to 10^{35} cm^{-2}s^{-1}, referred to as "super-high" luminosity. Operation of CMS at super-high luminosity requires significant hardware upgrades [4].

Table 1. Expected luminosity at the LHC. The integrals assume running at 100% efficiency such that the last column is indicative of what might be expected per year.

	Instantaneous	*integral (1 month)*	*integral (4 months)*
low (initial)	2×10^{33} cm^{-2}s^{-1}	5 fb^{-1}	20 fb^{-1}
high (design)	10^{34} cm^{-2}s^{-1}	25 fb^{-1}	100 fb^{-1}
upgraded	10^{35} cm^{-2}s^{-1}	250 fb^{-1}	1000 fb^{-1}

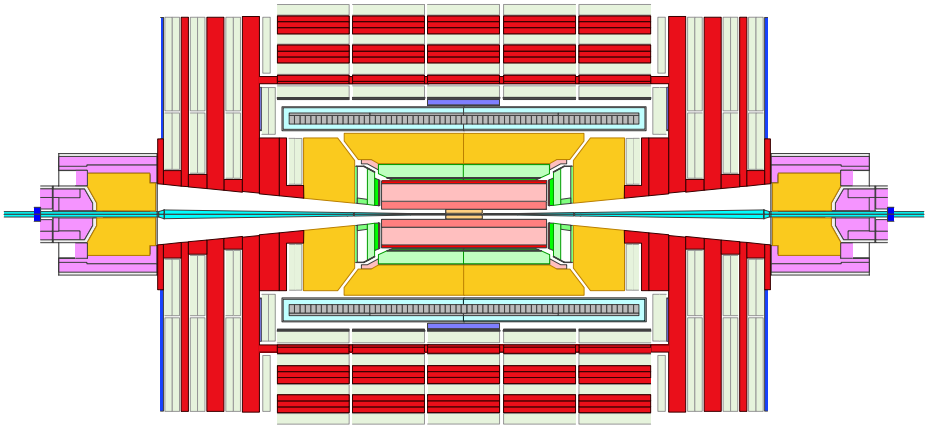

Fig. 2. The Compact Muon Solenoid detector, longitudinal view.

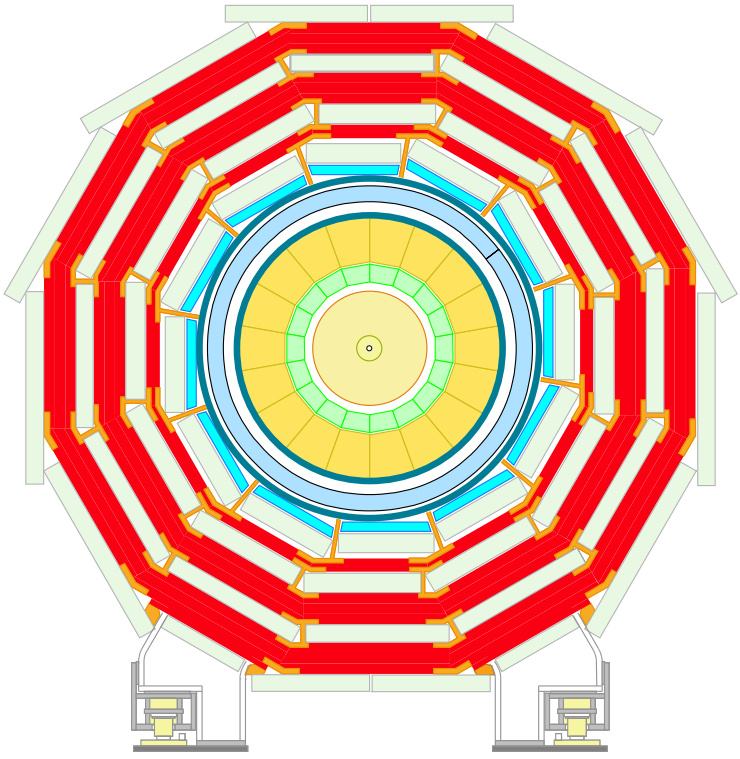

Fig. 3. The Compact Muon Solenoid detector, transverse view.

At high luminosity the proton-proton collision rate is about 800 MHz. The fundamental building blocks in the search for new physics, the W and Z bosons, are produced at a rate of about 1 kHz. The top quark, a major background to many of the processes presented in this paper, is produced at a rate of 10 Hz. Jets with TeV/c transverse momenta are copiously produced at a rate of about 1 Hz. Various TeV exotica, including the SM Higgs boson, supersymmetric particles, and new vector bosons may be expected at a rate of one every 15 minutes. The most energetic parton collisions, the events that will be used to justify the next accelerator, correspond to $x_{\mathrm{F}} = 1/2$ (parton energy divided by beam energy). The level-1 trigger hardware has a maximum output of 100 KHz and the high-level trigger a maximum output of 100 Hz [5]-[6].

1.2 Simulation and Reconstruction

The calculation of the physics reach at the LHC has become a cottage industry. True reach involves many subtleties: trigger, detector resolution and efficiency, event pileup, and the ubiquitous QCD backgrounds (which always seem to be underestimated!). For the processes discussed in this paper, event generation is performed with PYTHIA, and reconstruction is done using a fast tracker simulation which has been compared to a detailed simulation (Fig. 5). Where appropriate, event pile-up corresponding to high or super-high luminosity has been included.

2 Standard Model Higgs Boson

The Higgs sector in the context of the standard model and beyond has been thoroughly evaluated theoretically [7]. The cross section for the SM Higgs boson, shown in Fig. 6 for next-to-leading order, is dominated by gluon fusion. Figure 7 shows the branching ratios and total width *vs.* Higgs boson mass. In the following sections, recent work on the channels qqH (W fusion), $\mathrm{t\bar{t}H}$), and WH is addressed. These channels complement searches in the channels $\mathrm{H} \rightarrow \mathrm{WW}^{*}$ and $\mathrm{H} \rightarrow \gamma\gamma$ and have competitive sensitivities due to background rejection introduced by tagging the associated forward jets, top quarks or W bosons, respectively.

2.1 WW Fusion

An important channel for detection of a light Higgs boson is the production by vector-boson fusion [9], as indicated in Figure 8, with both W bosons decaying leptonically. The main background to this channel is $\mathrm{t\bar{t}}$ production which provides a copious source of events with two W bosons in the final state. The presence of two forward jets ($p_{\mathrm{T}} > 20$ GeV/c) at large pseudorapidity ($|\eta| > 4.3$) in opposite ends of the detector ($m_{\mathrm{jj}} > 600$ GeV/c^2), provides a high-efficiency event tag which reduces the top-quark background by an order of magnitude, thereby compensating for the lower fusion cross section. Other key selection cuts are an anti-b tag using charged particle impact parameter [10], two isolated high-p_{T} leptons ($p_{\mathrm{T}} > 20$ GeV/c) with $m_{\ell\ell} < 60$ GeV/c^2 and $\Delta\phi < 140^{\circ}$, and a veto

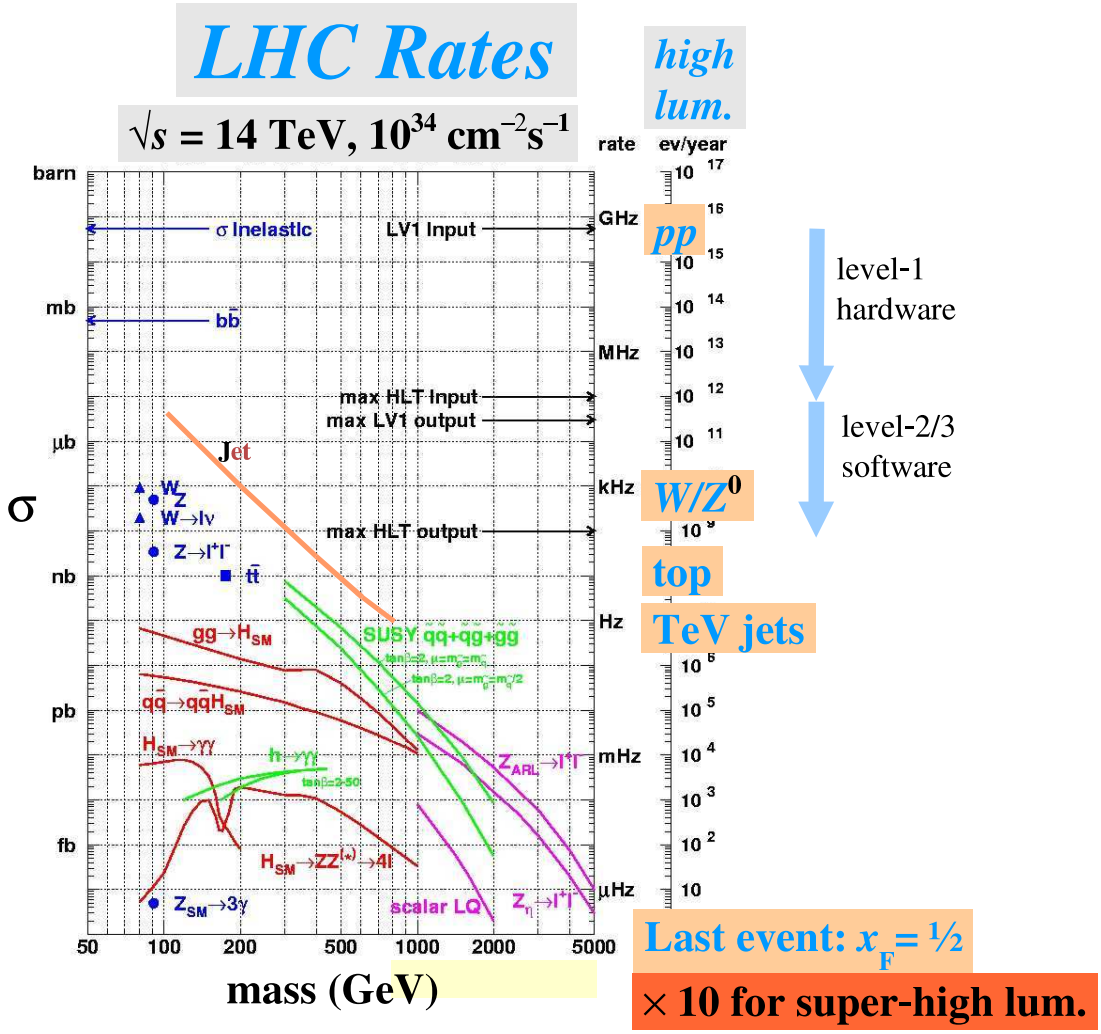

Fig. 4. LHC rates.

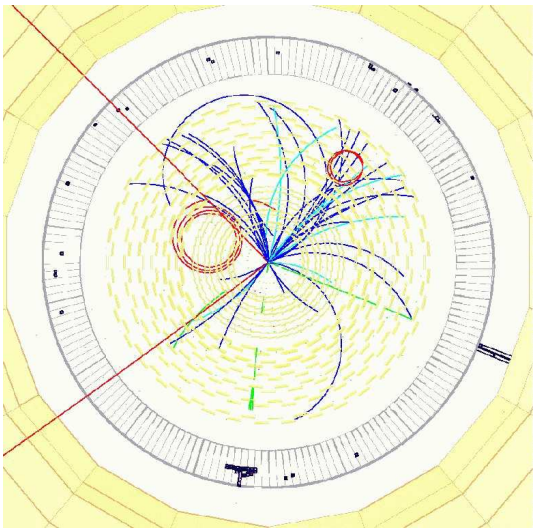

Fig. 5. Simulated and reconstructed CMS event, $H \to ZZ \to e^+e^-\mu^+\mu^-$.

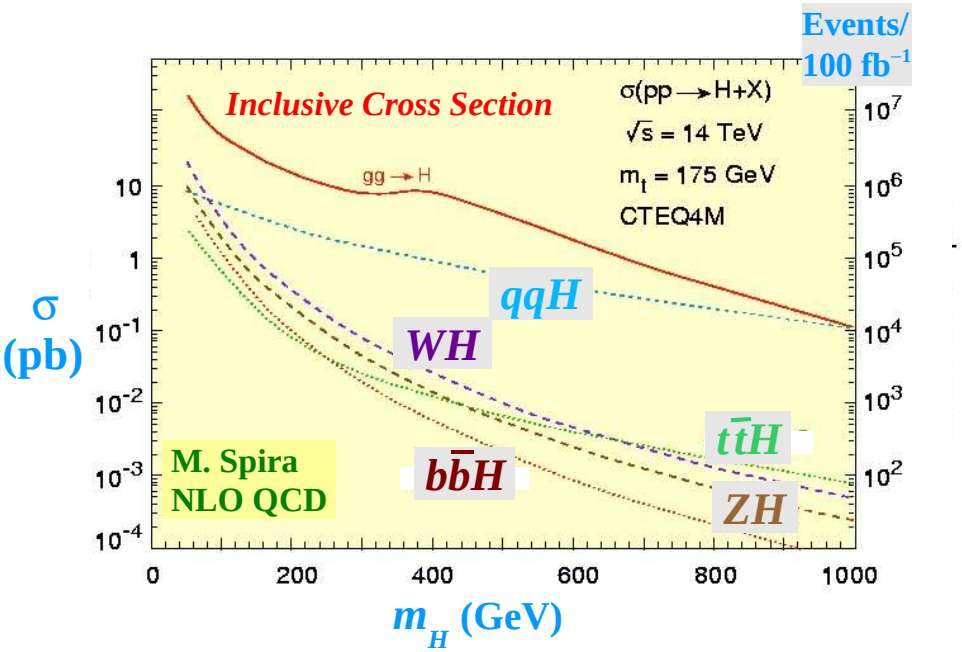

Fig. 6. Standard model Higgs boson production cross sections at the LHC calculated in next to leading order QCD [8].

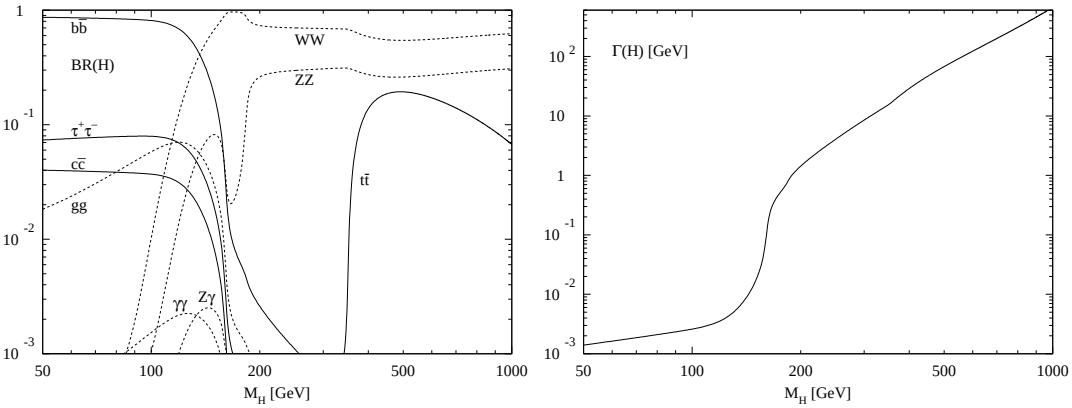

Fig. 7. Left: Branching ratios for the SM Higgs boson. Right: Total decay width [8].

on additional jets with $p_{\mathrm{T}} > 20$ GeV/c. At a Higgs boson mass of 120 GeV/c^2, the signal starts to emerge (220 signal events on top of a background of 680 events for an integrated luminosity of 100 fb^{-1}), while at higher mass the signal becomes striking as shown in Fig. 9.

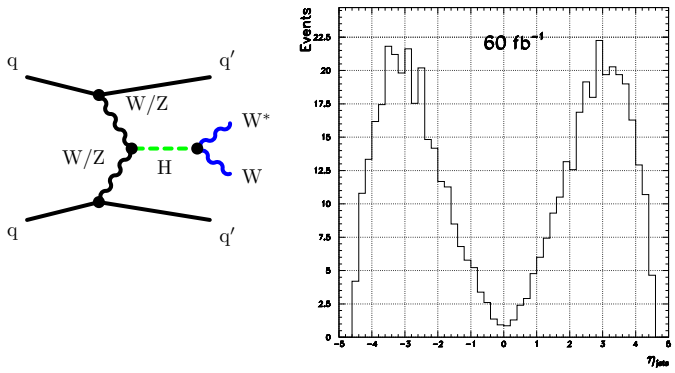

Fig. 8. Left: Diagram for Higgs boson production by vector-boson fusion. Right: Rapidity distribution of quark jets from the vector-boson fusion process [9]. Forward calorimetry is important for tagging these jets.

2.2 Radiation From Top (t$\bar{\mathrm{t}}$H)

Another interesting production channel for the SM Higgs boson is via radiation from a top quark (t$\bar{\mathrm{t}}$H) [11],[12] as indicated in Fig. 10. A Higgs boson decay into b$\bar{\mathrm{b}}$, together with the top decays, $\mathrm{t} \to \ell^+\nu\mathrm{b}$ and $\bar{\mathrm{t}} \to \mathrm{q}\bar{\mathrm{q}}\bar{\mathrm{b}}$ (or conjugate states), gives an event signature of four b-quark jets. The b quarks have favourable transverse energy (E_{T}) and rapidity distributions for secondary vertex tagging

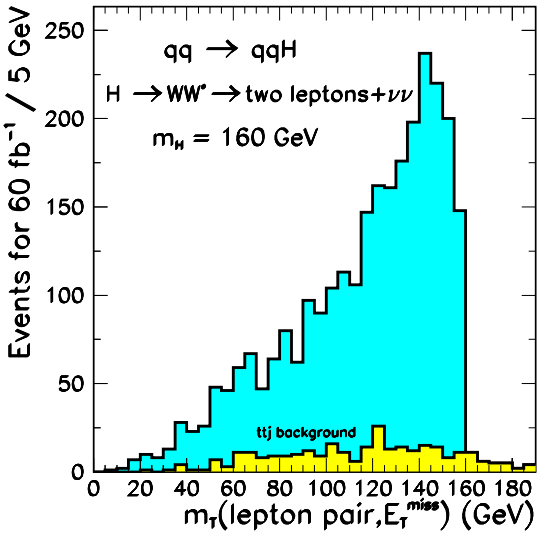

Fig. 9. Reconstructed transverse mass from lepton-lepton-missing E_T for a 160 GeV/c^2 Higgs boson produced by vector-boson fusion and $t\bar{t}$ background for an integrated luminosity of 60 fb^{-1}. The study was done with fast simulation.

(Fig. 10). The b-tagging procedure is described in Ref. [10]. A lepton tag from one of the W bosons from top decay, a two-jet constraint to the W mass from the other top decay, plus two top-mass constraints ($q\bar{q}\bar{b}$ and $\ell^+\nu b$) give an an overall efficiency of 1.3%, while the main backgrounds from $t\bar{t}b\bar{b}$ and $t\bar{t}Z$ are rejected by factors of 250 and 500, respectively.. The resulting jet-jet ($b\bar{b}$) mass distribution is shown in Fig. 11 for a Higgs boson mass of 115 GeV/c^2 and an integrated luminosity of 30 fb^{-1} [12]. This illustrates the figure of merit for hadronic calorimetry at the LHC, namely, the jet-jet mass resolution which governs the ability to do parton spectroscopy. The resulting mass resolution is a rather subtle combination of detector energy resolution and segmentation as well as quantum fluctuations of the parton fragmentation process. The jet-jet mass resolution in the region of 100 GeV/c^2 is about 12%.

2.3 WH Production

Figure 12 shows the Feynman diagram for a Higgs boson radiated from a W, with subsequent decay into $b\bar{b}$, giving an $\ell^{\pm}\nu b\bar{b}$ final state. The cross section for this process is about 1.5 pb for a Higgs boson mass of 115 GeV/c^2. There are enormous backgrounds, however, from $t\bar{t}$ (570 pb), $t\bar{b}$ (320 pb), Wjj (30 pb), and WZ (27 pb). The tagging of the two b's, as well as the charged lepton from the W decay, is critically important for the extraction of the signal. Figure 12 shows the background-subtracted signal expected for 300 fb^{-1} and a Higgs boson mass of 115 GeV/c^2.

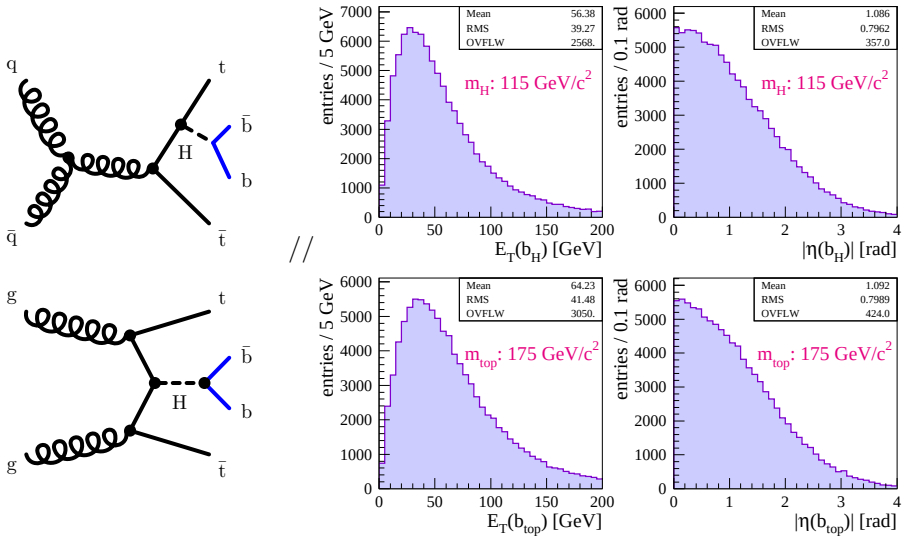

Fig. 10. Left: Representative diagrams for SM Higgs boson production via radiation from a top quark and decay into b quarks. Right: Transverse energy and rapidity distributions of b quarks produced in the process $t\bar{t}H \rightarrow W^+bW^-\bar{b}b\bar{b}$ for a 115 GeV/c^2 Higgs boson mass (upper) and a 175 GeV/c^2 top-quark mass (lower) [12].

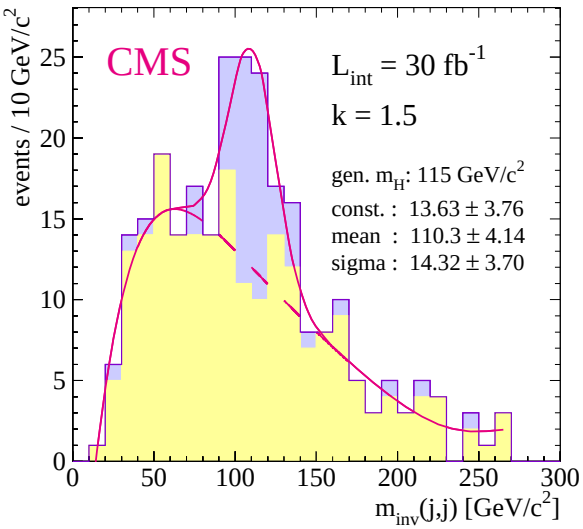

Fig. 11. Reconstructed jet-jet mass for a 115 GeV/c^2 SM Higgs boson produced in association with a top quark pair and decaying into $b\bar{b}$ for 30 fb $^{-1}$ [12]. The study was done with fast simulation.

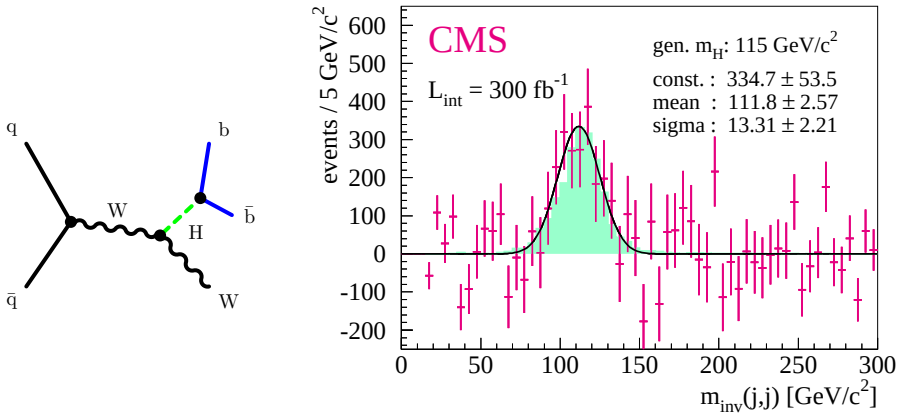

Fig. 12. Left: Higgs boson production via radiation from a W boson. Right: Reconstructed jet-jet mass for a 115 GeV/c^2 Higgs boson produced in association with a W and decaying into $b\bar{b}$ for 300 fb^{-1} [13]. The study was done with fast simulation and high-luminosity event pile-up.

Although not expected to be an early discovery mode for a light Higgs boson, the WH channel is independent of the top quark and provides an interesting measurement of the WWH coupling as indicated in Fig. 13. Measurement of this coupling assumes that the branching ratio, H $\rightarrow$ $b\bar{b}$ is known.

2.4 Warhorses

The production of SM Higgs bosons by gluon fusion and the decays to $\gamma\gamma$ or ZZ $\rightarrow \ell^+\ell^-\ell^+\ell^-$ or $\ell^+\ell^-\nu\nu$, and production by W fusion with decay into $W^+W^- \rightarrow \ell^+\nu\ell^-\nu$ or $\ell^{\pm}$jj have served as benchmarks for the design of CMS [1]. These warhorses have been talked about extensively at many conferences and there is nothing new to report; some characteristic mass plots (Fig. 14) are included here for reference.

2.5 Limits

Figure 15 shows the expected sensitivity in CMS for the SM Higgs boson, expressed as the statistical significance of the signal (σ) *vs.* Higgs boson mass for an integrated luminosity of 100 fb^{-1}. Above some threshold of many standard deviations, the Higgs boson should be observable and there is little difference at this stage between predicting 10σ and 30σ signals! The main point is that the channels presented in the previous section, qqH, WH, and $t\bar{t}H$ provide important redundancy to the potential discovery at low mass where the $\gamma\gamma$ mode presents a huge experimental challenge. The hardest part will be to find the first signal. When the mass is known and QCD backgrounds are measured, it will be comparatively easy to observe the Higgs boson in additional decay channels.

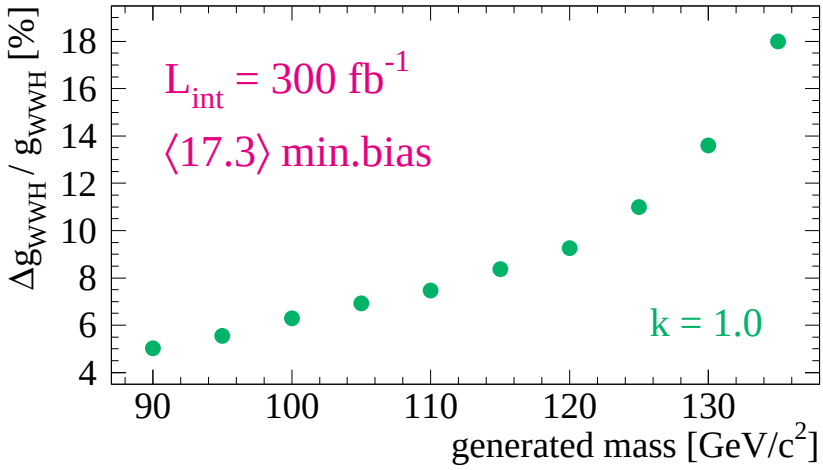

Fig. 13. Predicted precision in measurement of the WWH coupling for Higgs bosons produced in association with W bosons for 300 fb^{-1}, assuming the branching ratio, H → b$\bar{\text{b}}$ is known [13].

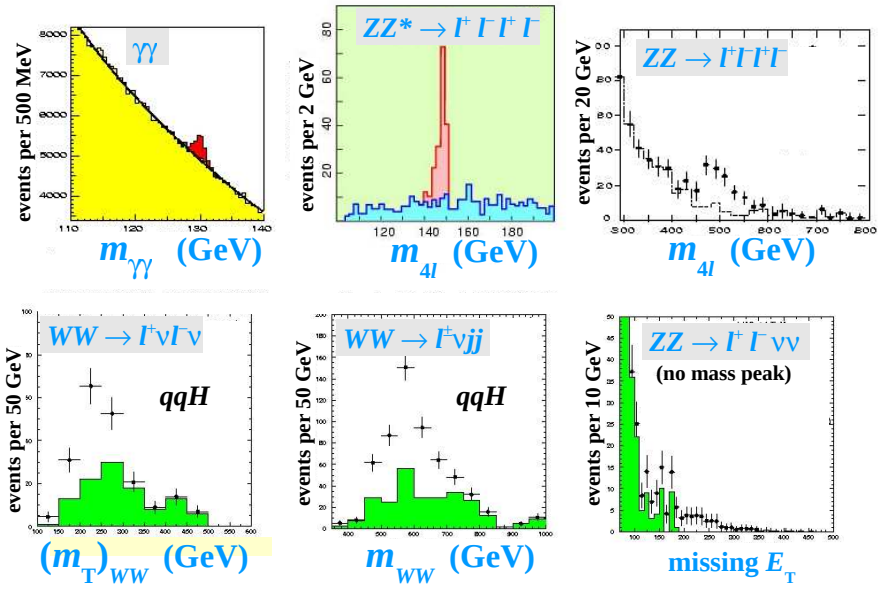

Fig. 14. CMS SM Higgs boson warhorses (clockwise from upper left): H → γγ, H → ZZ → 4ℓ (low mass), H → ZZ → 4ℓ (high mass), H → W$^+$W$^-$ → $\ell^+\nu\ell^-\bar{\nu}$, H → W$^+$W$^-$ → $\ell^\pm\nu$jj, H → ZZ → $\ell^+\ell^-\nu\bar{\nu}$ [14],[15]. The plots were made using fast simulation.

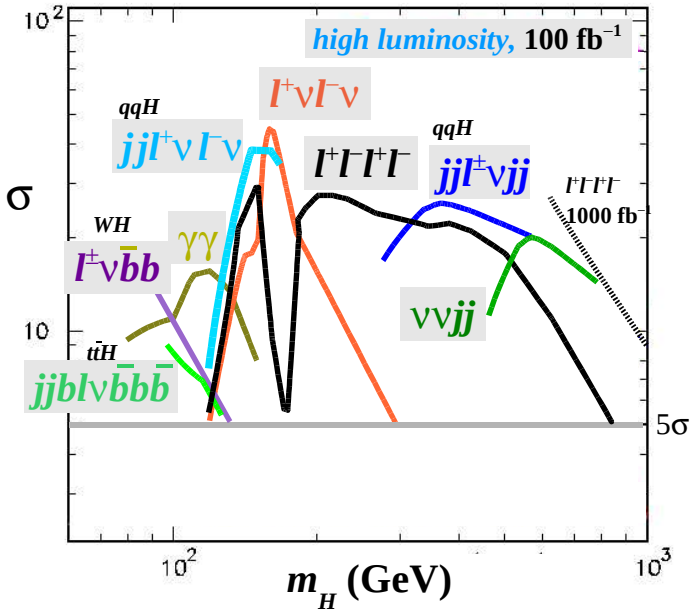

Fig. 15. Coverage in CMS for the SM Higgs boson expressed as the signal significance (σ) *vs.* mass for 100 fb^{-1}. The SM Higgs boson is expected to be observable in multiple decay modes over the entire mass range.

3 Minimal Supersymmetric Standard Model Higgs Bosons

Supersymmetry would greatly enrich the Higgs-sector [7],[16], requiring the presence of at least two Higgs doublets, in contrast to only one in the SM. After three degrees of freedom are taken to give mass to the W and Z bosons, five physical states remain: two scalars (h and H), one pseudoscalar (A), and two charged Higgs (H^+ and H^-).

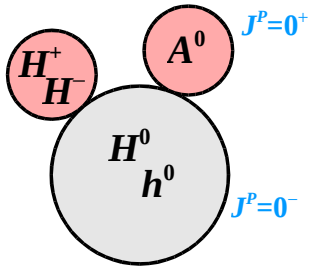

Fig. 16. The minimal supersymmetric extension of the standard model leads to a three-ring circus of Higgs bosons.

The lighter scalar h is predicted to have a mass below 130 GeV/c^2 such that the limits on supersymmetry from LEP are substantial [17]. Supersymmetry

stays alive by going to that corner of parameter space with maximal stop mixing (Fig. 17) and large tanβ, the standard parameter that specifies the ratio of vacuum expectation values of the two Higgs boson doublets [7]. The relationship between the masses (H, A, and $H^{\pm}$) for tanβ=3 and tanβ=30 is indicated in Fig. 17.

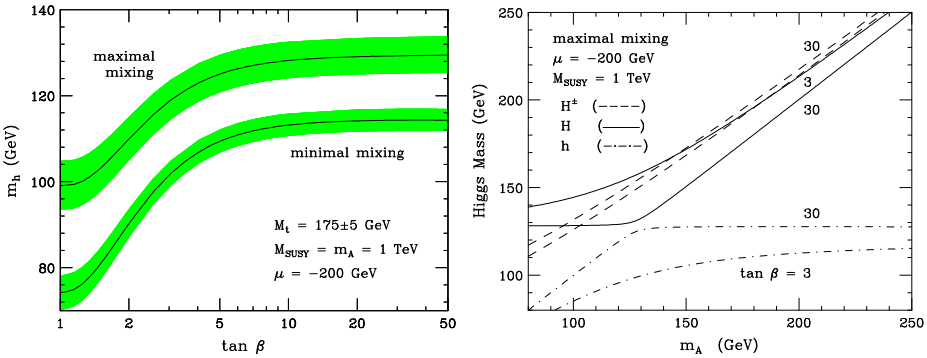

Fig. 17. Left: MSSM Higgs boson (h) mass vs. tanβ for minimum and maximum stop mixing. Right: Higgs boson (h, H, $H^{\pm}$) masses vs. m_A for two different values of tanβ [18].

3.1 Decays into Taus

The dominant mechanism for production of MSSM Higgs bosons is radiation from b quarks. Figure 18 shows the MSSM cross section and branching ratios for tanβ=30. The coupling of H and A to tau leptons (and also to b quarks) grows in proportion to tanβ. Thus, the large values of tanβ implied by LEP data make Higgs boson decays into taus an important channel (Fig. 19) [19]. Leptonically decaying tau pairs producing e^+e^- or $\mu^+\mu^-$ suffer from a huge Drell-Yan background, but signals are predicted to be observable in the electron-muon, lepton-jet, and jet-jet final states. The following three subsections correspond to the production $b\bar{b}H$ as indicated in Fig. 19.

3.1.1 $H \rightarrow \tau^+\tau^- \rightarrow e\mu$. For the electron-muon channel, events are selected with an isolated electron and muon with $p_T > 20$ GeV/c and $|\eta| < 2.5$. The isolation cut requires no charged particle track with $p_T > 2$ GeV/c in an η-ϕ cone of $\Delta R < 0.3$. Impact parameter cuts [10] on the leptons help reduce the main background arising from top and Z. A b-quark tag with $p_T > 2$ GeV/c reduces the background from W^+W^-. The result is shown in Fig. 20 for a Higgs boson mass of 200 GeV/c^2, with tanβ=20 and an integrated luminosity of 30 fb^{-1}

3.1.2 $H \rightarrow \tau^+\tau^- \rightarrow l^{\pm}$ + jet. For the lepton-jet decay, events are selected with an isolated high-p_T electron or muon, tau-jet selection (to reduce the background from b quarks), and a b-quark tag (to reduce the background from W

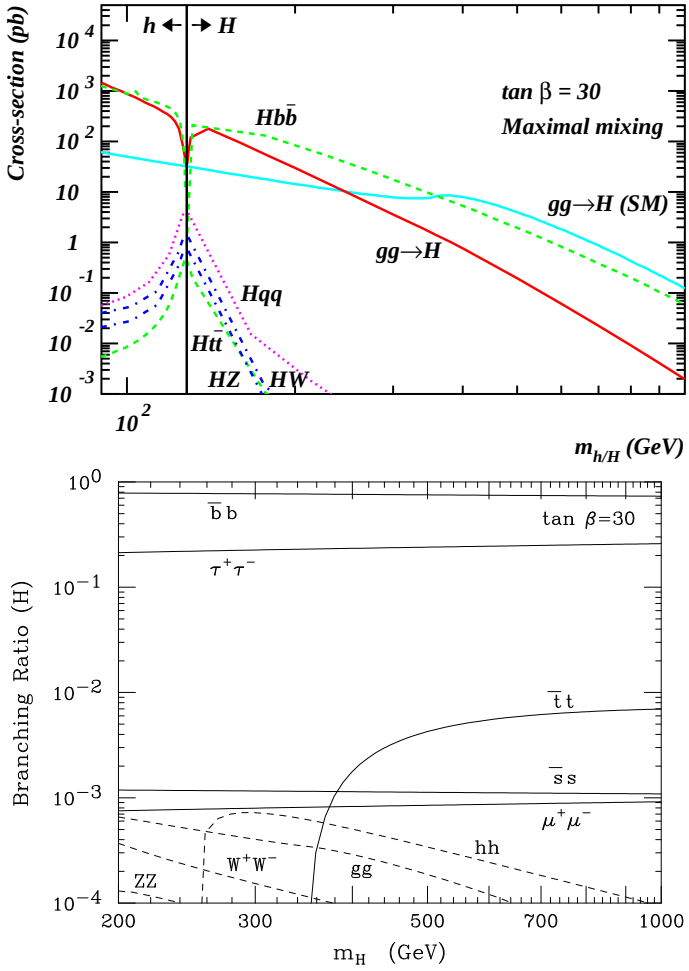

Fig. 18. Top: MSSM Higgs boson cross section for tanβ=30 and maximal stop mixing. Bottom: MSSM Higgs boson branching ratio [18].

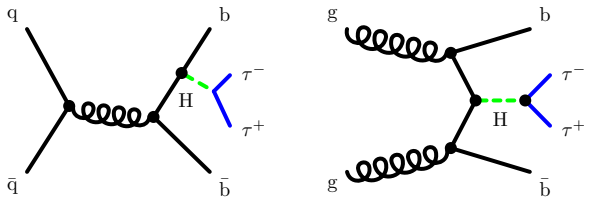

Fig. 19. Diagrams for MSSM Higgs boson production via radiation from a b quark and subsequent decay into taus.

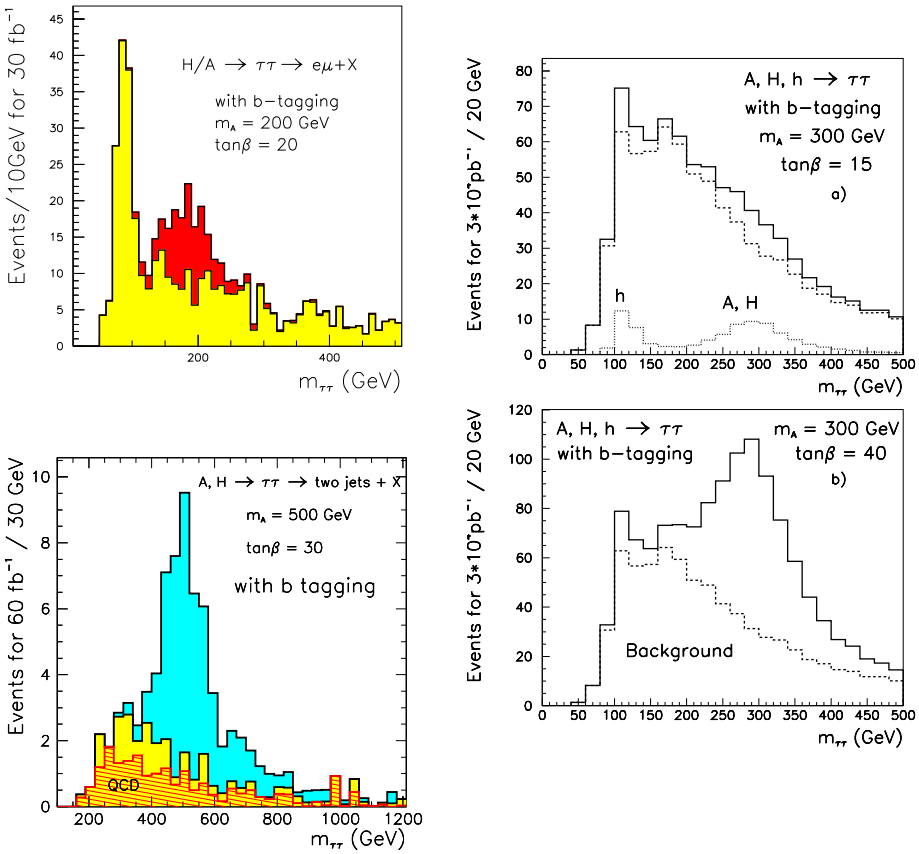

Fig. 20. Left upper: Electron-muon mass distribution for decay of MSSM Higgs bosons (H and A) to $\tau^+\tau^-$ with the taus decaying into electron and muon channels together with expected backgrounds. The plot is for $m_{\rm A}$=200 GeV/c^2, tanβ=20, and 30 fb^{-1} [20]. Right: Mass distribution for decay of H and A to $\tau^+\tau^-$ with one tau decaying into a lepton and another into hadrons. The plots are for $m_{\rm A}$=300 GeV/c^2 and 30 fb^{-1} and a) tanβ=15, b) tanβ=40 [21]. Left lower: Di-jet mass distribution for decay of H and A into $\tau^+\tau^-$ with both taus decaying into hadrons together with backgrounds from QCD and processes producing real taus. The plot is for $m_{\rm A}$=500 GeV/c^2, tanβ=30 and 60 fb^{-1} [22]-[23]. The results were obtained using fast simulation with full event simulation for the impact parameter tagging.

and Z bosons). The result is shown in Fig. 20 for a Higgs boson mass of 300 GeV/c^2, two different values of tanβ (15 and 40), and an integrated luminosity of 30 fb^{-1}.

3.1.3 $\mathbf{H \rightarrow \tau^+\tau^- \rightarrow jet + jet}$. The background to the channel with two tau jets is dominated by QCD processes which fake the tau jets. The most effective cut is on the impact parameter of the two tau jets. Other cuts include the jet-jet azimuthal angle $\Delta\phi_{jj} < 178°$, b-quark tag with $p_T > 20$ GeV/c and a veto on additional jets. The background from events with real taus from W, Z, and top is irreducible and amounts to about 20% of the signal. The result is shown in Fig. 20 for a Higgs boson mass of 300 GeV/c^2, tanβ=30 and an integrated luminosity of 60 fb^{-1}.

3.2 Decays into Muons

Production of b$\bar{\text{b}}$H and decay of the MSSM Higgs boson into $\mu^+\mu^-$ (Fig. 21) are observable, in spite of the tiny 0.1% branching ratio (Fig. 18), because of the distinctive signature. The main background is from Drell-Yan. The signal for decays of H and A into $\mu^+\mu^-$ for m_A=150 GeV/c^2 and tanβ=30 together with the Drell-Yan and top-quark backgrounds for an integrated luminosity of 20 fb^{-1} are given in Ref. [2].

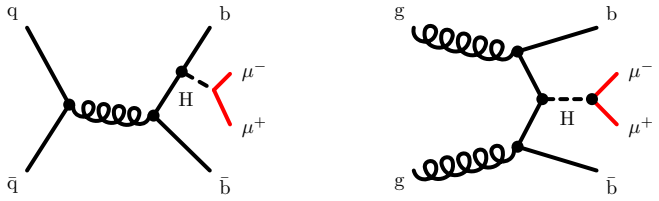

Fig. 21. Diagrams for MSSM Higgs boson production via radiation from a b quark and subsequent decay into muons.

3.3 Leptonic Decays via Neutralinos

An interesting MSSM Higgs boson signature arises from the production of b$\bar{\text{b}}$H and decay into two neutralinos ($\chi_2^0\chi_2^0$), if kinematically allowed, when the neutralinos each decay via sleptons ($\ell\tilde{\ell}$) as indicated in Fig. 22. The signature is four isolated, charged leptons with missing E_T. The resulting four-lepton mass distribution, shown for 100 fb^{-1} in Fig. 22, does not peak at the Higgs boson mass due to the large amount of missing energy, but there is essentially no background. The small amount of predicted background arises from other SUSY processes.

3.4 Charged Higgs Boson

A charged Higgs boson would be produced by radiation from a b quark, thereby producing an associated t quark. The CMS sensitivity to two decay modes, $H^- \rightarrow \bar{t}b$ ($H^+ \rightarrow t\bar{b}$) and $H^- \rightarrow \tau^-\bar{\nu}$ ($H^+ \rightarrow \tau^+\nu$), has been examined.

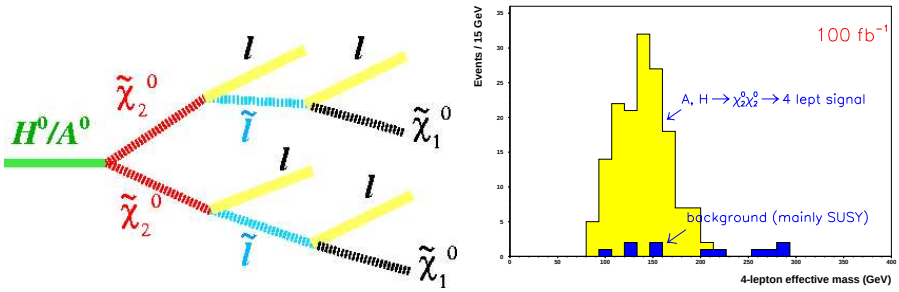

Fig. 22. Left: Decay of H/A via neutralinos and sleptons resulting in four charged leptons and missing E_{T}. Right: Four-lepton invariant mass distribution and background for 100 fb^{-1} and a 350 GeV/c^2 Higgs boson mass. The study was done with fast simulation.

3.4.1 Decay into $\mathrm{t\bar{b}}$. The H^+ (H^-) decay into $\mathrm{t\bar{b}}$ ($\mathrm{\bar{t}b}$) has a signature of three b-quark jets. The main background is from $\mathrm{t\bar{t}}$+jet with two real b jets and one mistagged jet. There is an additional background from $\mathrm{t\bar{t}b\bar{b}}$. The event selection requires a lepton from the top decay with $p_{\mathrm{T}} > 15$ GeV/c, five jets with $p_{\mathrm{T}} > 20$ GeV/c and $|\eta| < 2.4$, as well as the three b-quark tags. A mass constraint is placed on the semileptonic top-quark decay (Fig. 23). The invariant mass distribution for a 300 GeV/c^2 charged Higgs boson is shown in Fig. 23 for an integrated luminosity of 30 fb^{-1}. The background and signal have a similar shape which renders signal extraction difficult.

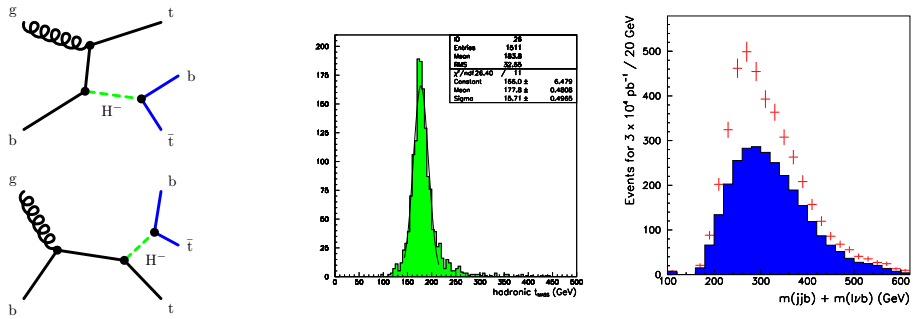

Fig. 23. Left: Diagrams for MSSM charged Higgs boson production with hadronic decay. Middle: Invariant mass of reconstructed top quarks. Right: Invariant mass of reconstructed charged Higgs boson and SM background for 30 fb^{-1} [24]. The results were obtained using fast simulation with full event simulation for the impact parameter tagging.

3.4.2 Decay into $\tau\nu$. Detection of the charged Higgs boson decay into $\tau\nu$ is more promising. The τ is required to have transverse energy greater than 100 GeV and have consistency between the measured track and calorimeter energies ($pc/E > 0.8$). In addition, the missing transverse energy is required to be greater than 100 GeV, and there must be three jets (from the top quark decay) with $E_{\mathrm{T}} > 20$ GeV. The mass of two of these jets must match the W mass to within 15 GeV/c^2 and the third jet must be tagged as a b quark. The mass of all three jets must match the top mass to within 20 GeV/c^2. Finally, the azimuthal angle between the tau and the missing transverse energy must be greater than 60°. The resulting invariant mass distribution for a 400 GeV/c^2 charged Higgs boson and tanβ=40 is shown in Fig. 24 for an integrated luminosity of 60 fb^{-1}. Due to the large missing energy, the events do not peak at the Higgs boson mass; however, the background peaks near the W mass, resulting in a clean signature.

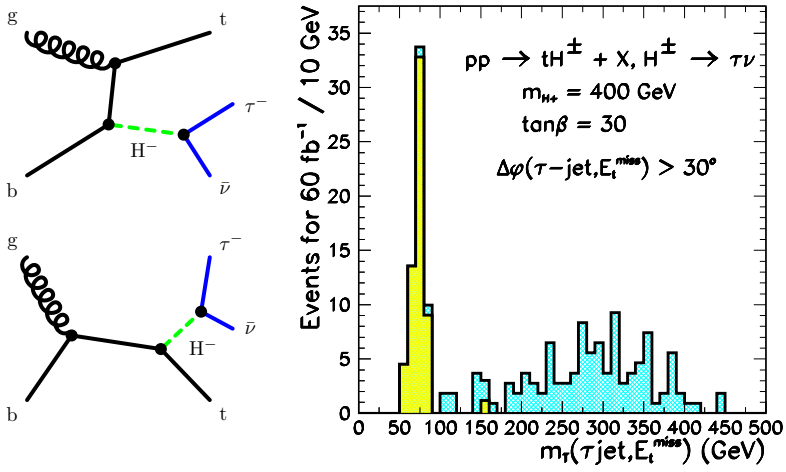

Fig. 24. Left: Diagrams for MSSM charged Higgs boson production with leptonic decay in the tau channel. Right: Invariant mass distribution of the tau jet plus missing E_{T} together with SM backgrounds which are dominated by events with W bosons, giving the low energy peak [25]. The results were obtained using fast simulation with full event simulation for the impact parameter tagging.

3.5 Limits

Figure 25 shows the expected sensitivity in CMS for the MSSM Higgs boson expressed as coverage in the m_A,tanβ plane. The limits correspond to 100 fb^{-1}, except for the tau limits involving jets which correspond to 30 fb^{-1}. The insensitivity to the region of high mass and low values of tanβ is due to the small coupling of H and A to b quarks and the small production cross sections.

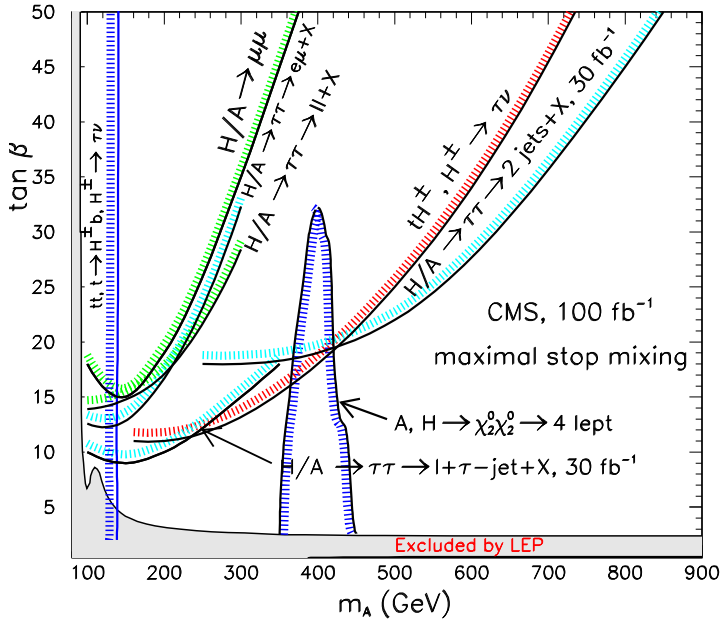

Fig. 25. Coverage for the MSSM Higgs boson in the m_{A},tanβ plane.

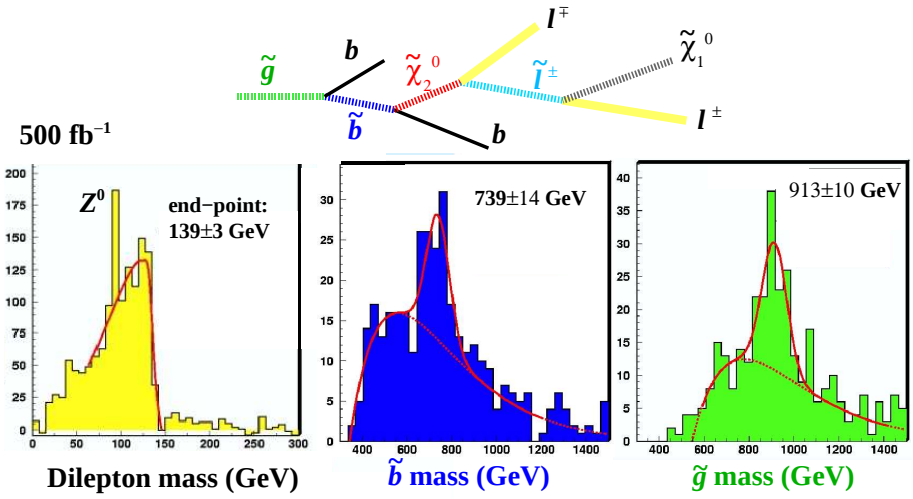

Fig. 26. Top: Gluino decay chain producing b quarks and charged leptons. Left: Reconstruced di-lepton mass. Center: Reconstructed b-squark mass. Right: Reconstructed gluino mass. The event reconstruction is done with fast simulation and corresponds to an integrated luminosity of 500 fb^{-1} [27].

4 Sparticle Search

If supersymmetry exists, the spectrometry will be so rich and complicated [26] that it may take decades to sort out. In the minimal supergravity model (mSUGRA) the breaking of supersymmetry is mediated by gravity. Production of SUSY particles is dominated by squarks and gluons with picobarn cross sections at TeV/c^2 masses (Fig. 4). Events are distinguished from SM processes by the multiple jets with large missing E_{T} and large missing transverse energy carried away by stable neutralinos. The presence of one or more leptons further aids in the interpretation of the events.

4.1 Squark and Gluino Reconstruction

In mSUGRA models, the lightest supersymmetric particle (LSP) is the lightest neutralino, ${\chi_1}^0$, which is stable. One of the most powerful, early signatures of sparticles is from the decay chain ${\chi_2}^0 \rightarrow \ell^-\tilde{\ell}^+ \rightarrow \ell^-{\chi_1}^0\ell^+$ as indicated in Fig. 26. The dileption mass has a well-known kinematic "edge" [27],[28] as indicated in Fig. 26 for a ${\chi_2}^0$ mass of 140 GeV/c^2. If the mass of the LSP is known (or the ratio of the mass of ${\chi_2}^0$ to that of the ${\chi_1}^0$ is known), the sparticle masses may be reconstructed [27]. Combining the results of the edge fit with a tagged b-quark jet gives the reconstructed b-squark mass (739 ± 14 GeV/c^2) shown for an integrated luminosity of 500 fb^{-1}. Further combination of the reconstructed b squark with a second b-quark jet gives the reconstructed gluino masses of 913 ± 10 GeV/c^2.

4.2 Limits

Figure 27 summarizes the expected sparticle mass reach expressed in the mSUGRA scalar-gaugino and gluino-squark mass planes. The SUSY gaugino/scalar mass reach is about 1.2 TeV/c^2 for 100 fb^{-1}, extending to about 1.4 TeV/c^2 for 1000 fb^{-1}. The gluino/squark reach is about 2.5 TeV/c^2 for 100 fb^{-1}, extending to about 3 TeV/c^2 for 1000 fb^{-1}.

5 Graviton

Superstring models of particle physics have dimensions beyond the usual 3+1 space-time. There are several models with quite different phenomenologies that exploit the geometry of space-time to solve the hierarchy problem. In the Randall-Sundrum model [29], warped extra dimensions lead to massive Kaluza-Klein graviton excitations that are produced by quarks or gluons and decay into pairs of jets, leptons or photons, producing a spectacular experimental signature (Fig. 28).

Figure 29 shows the reconstructed $\mathrm{e}^+\mathrm{e}^-$ and $\mu^+\mu^-$ mass distributions for a 3 TeV/c^2 graviton resonance using full event simulation. The main SM background is the production of dileptons via the Drell-Yan mechanism. In this mass region there is almost no background and event pile-up is not an issue.

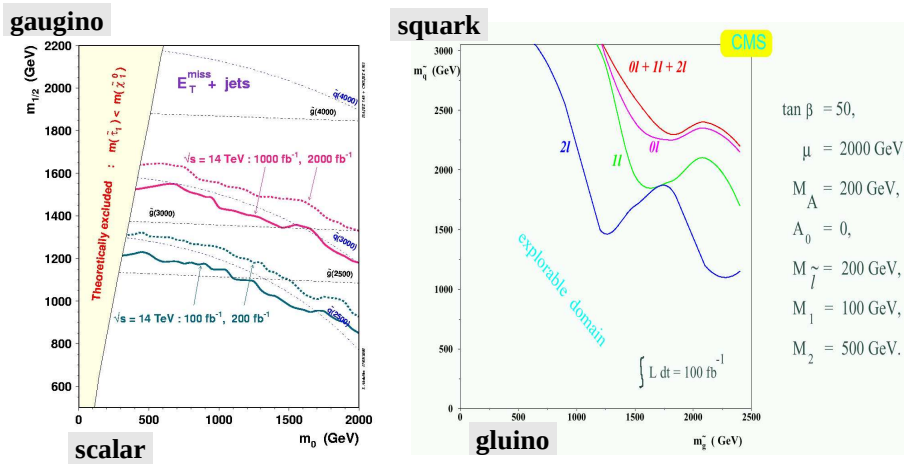

Fig. 27. Sparticle mass reach.

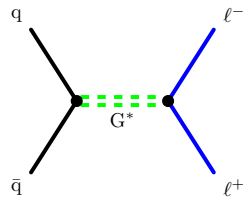

Fig. 28. Kaluza-Klein graviton excitation.

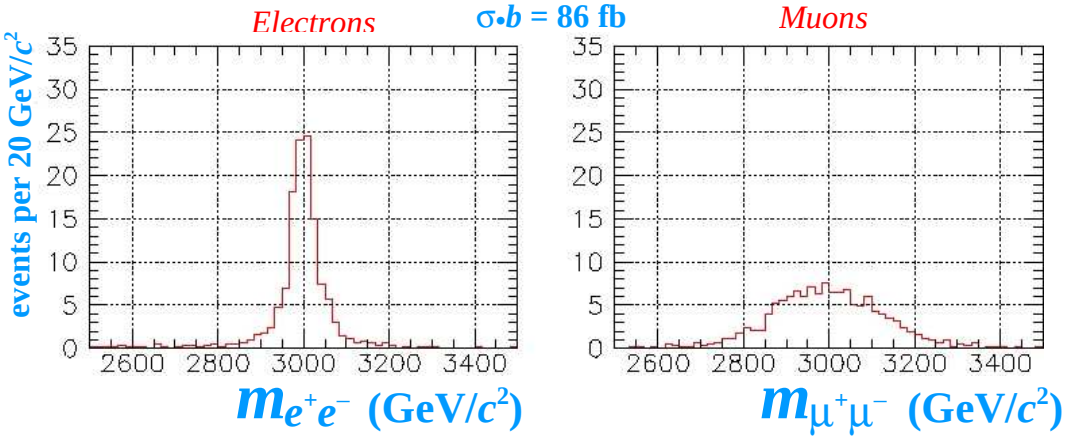

Fig. 29. Left: Reconstructed e^+e^- mass for a 3 TeV/c^2 resonance. Right: Reconstructed $\mu^+\mu^-$ mass for a 3 TeV/c^2 resonance. This is a first, preliminary calculation using fast simulation [30].

Figure 30 shows the expected sensitivity in terms of graviton coupling strength (vertical axis) vs. mass (horizontal axis) for 100 fb^{-1}. The interesting region is bounded by consistency with Newton's Law ($|R_5| < {M_5}^2$) and ability of the model to solve the hierarchy problem ($\Lambda_d < 10$ TeV) for which it was invented in the first place. The theorists will no doubt invent more sophisticated versions that are harder to detect or rule out.

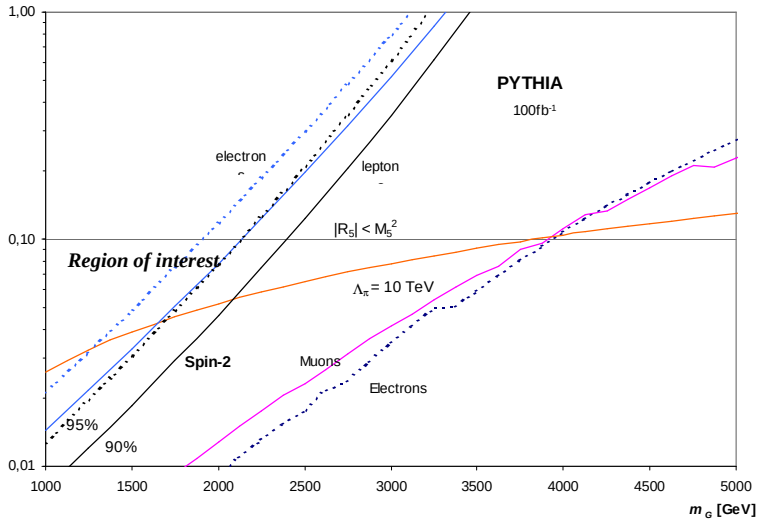

Fig. 30. Limits on Kaluza-Klein graviton excitations in the Randall-Sundrum model for e^+e^- and $\mu^+\mu^-$ channels [30]. The region above the curves labeled Muons, and Electrons can be ruled out with an integrated luminosity of 100 fb^{-1}. The curves on the left show the 90% and 95% confidence levels for distinguishing spin 2 from spin 1.

6 New Heavy Vector Boson

New gauge bosons, W′ and Z′, are allowed by superstring theories. A new heavy vector boson is expected to be produced by the Drell-Yan mechanism (Fig. 31) so that decay into e^+e^- or $\mu^+\mu^-$ pairs provides a powerful experimental signature. The rates depend on the coupling strength. The current limit on a new W′ from the Tevatron is about 720 GeV/c^2, assuming SM couplings [31]. Detection of new gauge bosons decaying into two jets is more difficult experimentally, but the rates are much larger [5].

The experimental signature of high-mass e^+e^- or $\mu^+\mu^-$ pairs is similar to that described in the previous section for the Kaluza-Klein graviton excitation (Fig. 29). The backgrounds are estimated to be very small (about 2% from non-resonant Drell-Yan and 1% from top). The number of expected events for a Z′ with SM couplings corresponding to an integrated luminosity of 1000 fb^{-1} is indicated in Fig. 31. Ten events are expected at a mass of about 6 TeV/c^2. For 100 fb^{-1}, ten events are expected at a mass of about 5 TeV/c^2.

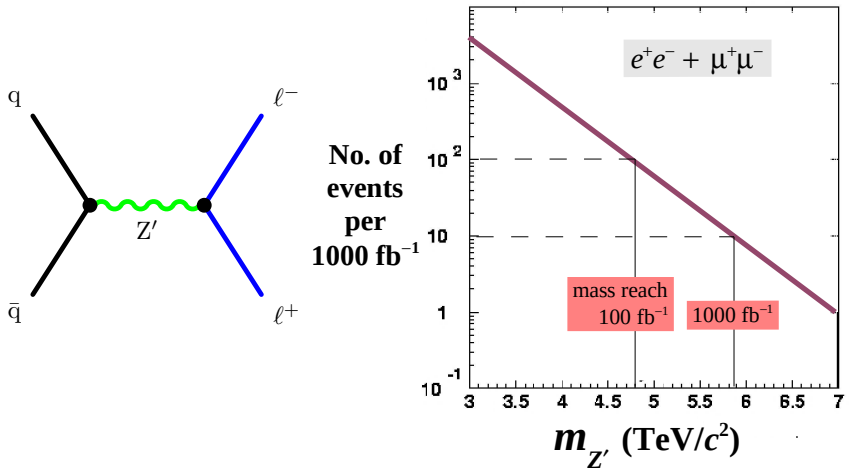

Fig. 31. Left: Feynman diagram for production of a new vector boson. Right: Number of Z' events expected in the e^+e^- and $\mu^+\mu^-$ channels (combined) for an integrated luminosity of 1000 fb^{-1} [34].

7 Summary of Mass Reach

The CMS mass reach for SM Higgs boson, SUSY, gravitons, and a new Z′ with SM couplings is shown in Fig. 32. Complete coverage over the mass range (0.1-1 TeV/c^2) is predicted for the SM Higgs boson at design luminosity. Mass reach for MSSM Higgs bosons and gauginos are predicted to approach one TeV/c^2 at design luminosity, extending to somewhat beyond at at super-high luminosity. The mass reach for graviton excitations and new gauge bosons approaches 5 TeV/c^2 at high luminosity, extending to nearly 6 TeV/c^2 at super-high luminosity. The figure of merit for a luminosity upgrade would be to extend the mass reach by approximately 20%.

8 Longitudinal Vector-Boson Scattering

If there is no light Higgs boson to tame the behaviour of the vector bosons at high energy, the unitary limit is reached at about 1.7 TeV. The W and Z bosons become strongly interacting and some new, unknown physics must appear, possibly well-below the unitary limit. Such a scenario has been previously encountered. The classical electron radius once imposed a formidable boundary at a distance scale of 3 fm, the "unitary" limit for the understanding of classical electrodynamics. Nothing special happens at the classical electron radius; indeed experiments have been performed at distance scales 1000 times smaller. The solution was the new physics discovered along the way, at much larger distance scales: quantum mechanics.

Longitudinal vector-boson scattering can produce resonance structure which may be observed by measuring pairs of W or Z bosons at high invariant mass [32]. Since such a resonance is produced by W or Z fusion, tagging of forward jets is an

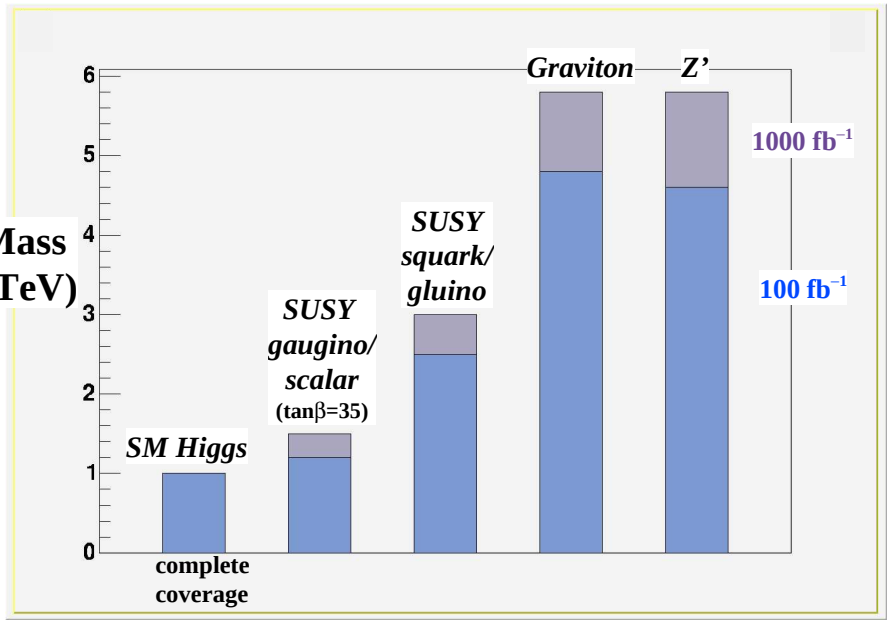

Fig. 32. Summary of CMS mass reach.

important part of the event signature (Fig. 8). Super-high luminosity is required to explore strongly interacting W and Z bosons with the LHC. More energy would be better [33]! Figure 33 shows one possible (optimistic?) scenario for detectable ZZ resonance structure from strongly interacting Z bosons with 3000 fb^{-1}. The event signature is four isolated leptons with forward and backward jets having energies greater than 400 GeV. The main background is qq $\rightarrow$ ZZ which has a cross section of about 9 fb for $m_{\mathrm{ZZ}} > 500\mathrm{GeV}/c^2$.

9 Compositeness

Models of compositeness are very difficult to build because any credible scenario has to account for the existing three families and the resulting myriad of particles, without introducing any extras.

If quarks and leptons are both composite and share the same constituents, compositeness causes a contact interaction as indicated in Fig. 34. This may be probed by searching for a deviation from lepton pairs produced by the Drell-Yan mechanism. An alternate technique, but more difficult experimentally, is to measure the angular distribution of jets. The latter method has the advantage of being independent of any possible lepton structure.

The contact interaction modifies the Drell-Yan cross section with the addition of a term proportional to $s/\alpha\Lambda^2$, where s is the dilepton invariant mass, α is the electroweak dimensionless coupling and Λ is the compositeness scale parameter. Figure 35 shows the effect of compositeness on the Drell-Yan cross section for various values of the parameter Λ. The present limit of about $\Lambda = 2$ TeV will

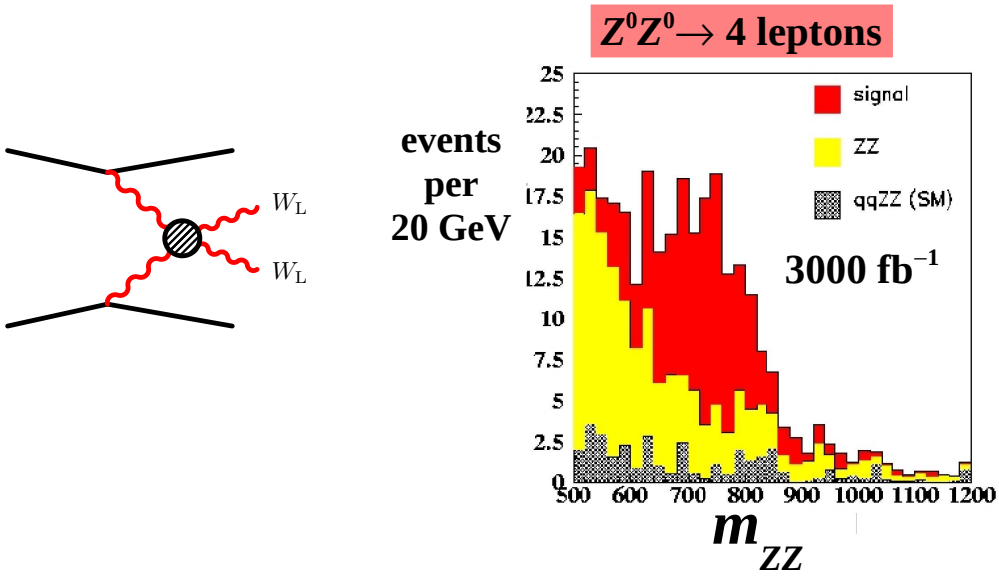

Fig. 33. Left: Diagram for longitudinal W/Z scattering. Right: Four-lepton mass (ZZ) due to possible resonance structure from strongly interacting Z bosons for an integrated luminosity of 3000 fb^{-1} [34]. The calculation was made using COMPHEP with CTEQ5L structure functions and implemented in PYTHIA for fast simulation.

be extended to about 30 TeV with 100 fb^{-1} and to 40 TeV with 1000 fb^{-1}.

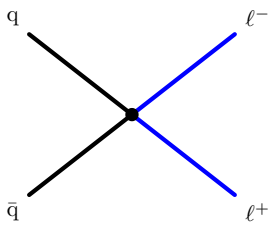

Fig. 34. Contact interaction caused by compositeness.

Compositeness has a rich history in particle physics. Rutherford discovered the nucleus using his famous 10 MeV alpha particles as probes [36]. Cockroft and Walton used 100 MeV protons to break apart the nucleus [37]. Hofstadter used 550 MeV electrons to observe that the proton had structure [38] which in turn lead to the deep inelastic experiments led by Friedman, Kendall, and Taylor that conclusively established the existence of quarks. These famous experiments spanned the 50 years that has been often referred to as the golden years of particle physics. The increase in energy that was needed to discover nucleons and quarks was only a factor of 60 beyond that needed to discover the nucleus! In the 1980s the UA1 and UA2 experiments at the CERN SPS Collider significantly

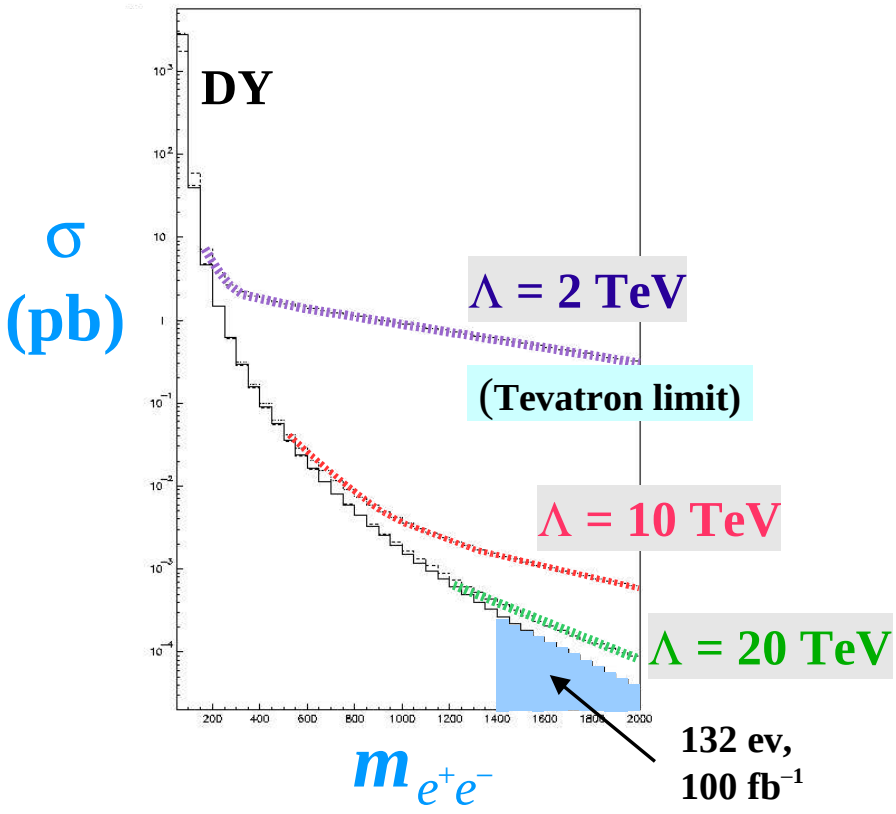

Fig. 35. Drell-Yan cross section *vs.* electron-positron mass [40]. The study was done with fast simulation.

extended this limit [39], LEP experiments added significantly to these searches, and the Fermilab Tevatron has pushed the limit up a bit further to about 400 GeV probe energy [40]. By the time the LHC comes into operation, 50 years will have passed since the discovery of proton structure and probes will be available with 10^4 times the energy of that time. From an experimentalist's point of view, this is exciting!

10 Summary and Outlook

The last invited talk I gave at Fermilab was twenty years ago at the 12th International Conference on High-Energy Accelerators, Aug. 11, 1983 [41]. This was a very exciting time in particle physics. The SPS Collider had allowed a huge step in centre-of-mass energy and the W and Z had finally been observed [42]. The Nobel prize for Carlo Rubbia and Simon Van der Meer was only a year away.

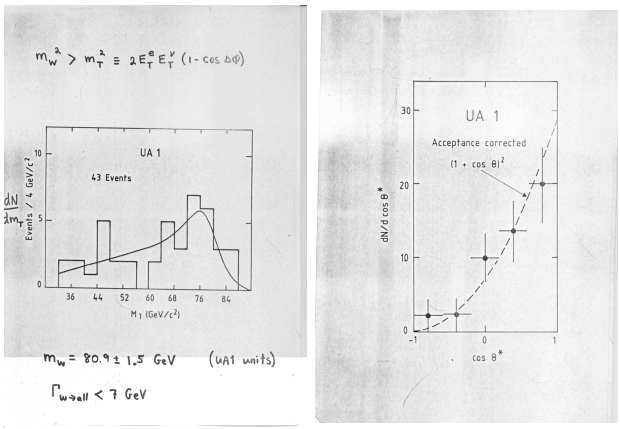

Fig. 36. Left: W mass fit to a statistical precision of 2% in 1983 with 42 events. Right: W spin determined to be $J = 1$ [41].

At the 1983 accelerator conference, Leon Lederman [43] quoted Tini Veltman from the 1982 SLAC Summer School:

The outstanding problems in today's theory of particles are such that none of the projections beyond the standard model can be considered with any confidence. What we need is experimental guidance: exposure to the no-man's land of lepton-lepton or quark-quark collisions up to the mass range of 1 TeV and beyond.

I thought it would be interesting to check with Tini to see how he felt about the progress in theoretical particle physics in the last twenty years. I got the following reply from him [44]:

Well, you know as well as I do that essentially nothing has changed. Supersymmetry and strings have not come closer to reality. The Higgs is more elusive than ever. I am happy to see that I saw that correctly in 1982.

We are, however, making progress [45]. In the two years since Sardinia, we have come at least one year closer to the realization of TeV physics! We seem to be now on track for 2007 to be a very exciting year in particle physics. When I

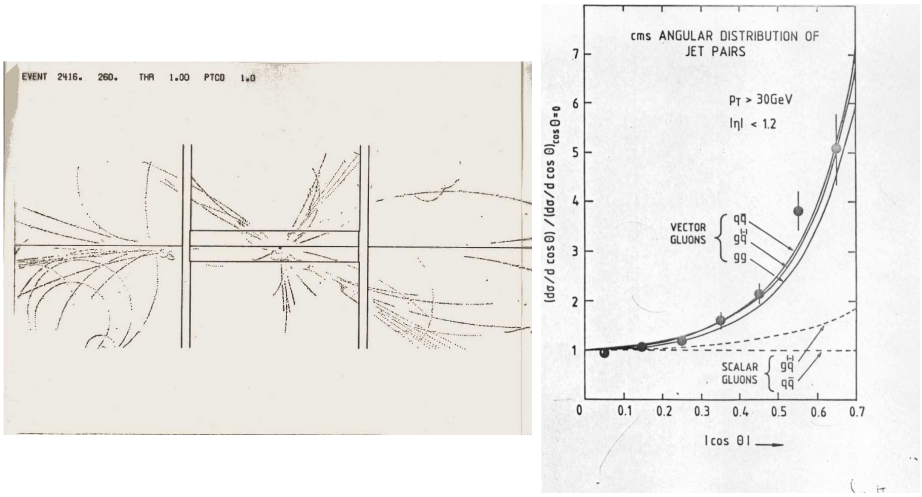

Fig. 37. Left: Jet event seen in the UA1 central tracking chamber. Right: Angular distribution of jets as living proof of asymptotic freedom, showing the gluon has $J = 1$ and the strong force behaves as $1/r^2$ at short distances [41].

get invited back to Fermilab in 2023, I hope to be able to report on some exciting new physics from CMS... that was NOT anticipated at this conference!

Acknowledgments

The following persons have made contributions to the preparation of this presentation: Daniel Denegri, Tini Veltman, Salavat Abdullin, Jack Gunion, Dan Green, Ritva Kinnunen, Sasha Nikitenko, Raman Sundrum, Grzegorz Wrochna, Alessia Tricomi, Wesley Smith, Stefano Villa, Sekhar Chivukula, Ken Lane, Tiziano Camporesi, Chiara Mariotti, Paris Sphicas, Patrick Janot, and Albert De Roeck.

References

1. The Compact Muon Solenoid, Letter of Intent, CERN/LHCC 92-3, LHCC/I 1, 1 October 1992.
2. The operation of the detector at turn-on luminosity of $2 \times 10^{33} \mathrm{cm}^{-2}\mathrm{s}^{-1}$ is described by K. Hoepfner, "Commissioning and Early Physics with CMS," *Proceedings of the IV International Symposium on LHC Physics and Detectors*, Fermilab (2003).
3. F. Ruggiero, "LHC Accelerator R&D and Upgrade Scenarios," *Proceedings of the IV International Symposium on LHC Physics and Detectors*, Fermilab (2003); O. Brüning et al., "LHC Luminosity and Energy Upgrade: A Feasibility Study," CERN-LHC-Project-Report-626, ed. F. Ruggiero (2002).
4. D. Green, "LHC Detector R&D, Upgrades and Extended Physics Reach," *Proceedings of the IV International Symposium on LHC Physics and Detectors*, Fermilab (2003).

5. CMS, The TriDAS Project, Technical Design Report, Volume 1: The Trigger Systems, CERN/LHCC 2000-38, CMS TDR 6.1, December 2000; CMS, The TriDAS Project, Technical Design Report, Volume 2: Data Acquisition and High-Level Trigger, CERN/LHCC 2002-26, CMS TDR 6.2, December 2002.
6. C. Seez, "The CMS Trigger System," *Proceedings of the IV International Symposium on LHC Physics and Detectors*, Fermilab (2003).
7. For a detailed recent summary, see J. F. Gunion, "Higgs Bosons in the Standard Model, the MSSM and Beyond," PASCOS03, Mumbai, January 2003.
8. M. Spira, "QCD Effects in Higgs Physics," hep-ph/9705337, *Fortsch. Phys.* **46** (1998) 203-284.
9. N. Akchurin *et al.*, "Study of Low-Mass Higgs Using pp → qqH at CMS," CMS Note 2002/016.
10. M. Mannelli, "CMS Inner Tracking," *Proceedings of the IV International Symposium on LHC Physics and Detectors*, Fermilab (2003).
11. D. Green, *et al.*, "A Study of $t\bar{t}$ + Higgs at CMS," CMS Note 2001/039.
12. V. Drollinger, Th. Muller, and D. Denegri, "Searching for Higgs Bosons in Association with Top Quark Pairs in the H → $b\bar{b}$ Decay Mode", CMS Note 2001/054, hep-ph/0111312.
13. V. Drollinger, Th. Muller, and D. Denegri, "Prospects for Higgs Boson Searches in the Channel $W^{\pm}H \to \ell^{\pm}\nu b\bar{b}$", CMS Note 2002/006, hep-ph/0201249.
14. CMS, The Electromagnetic Calorimeter Project: Technical Design Report, CERN/LHCC 97-33 CMS TDR 4, 364 pages, December 1997.
15. M. Dittmar and A. Nicollerat, "High-Mass Higgs Studies Using gg → qqH at the LHC," CMS Note 2001/036.
16. E. Witten, "Prospects for Future Discoveries," ICFA Seminar, CERN, Oct. 8, 2002.
17. The ALEPH, DELPHI, L3 and OPAL Collaborations and the LEP Higgs Working Group, "Searches for the Neutral Higgs Bosons of the MSSM: Preliminary Combined Results Using LEP Data Collected at Energies up to 209 GeV," hep-ex/0107030, CERN-EP/2003-011, submitted to *Phys. Lett.*
18. M. Carena and H. E. Haber, "Higgs Boson Theory and Phenomenology," hep-ph/0208209, *Prog. Part. Nucl. Phys.* **50** (2003) 63.
19. S. Eno *et al.*, "A Study of a First and Second Level Tau Trigger," CMS Note 2000/055; D. Kotliński *et al.*, Study of a Level-3 Tau Trigger with the Pixel Detector," CMS Note U2001/017; A. Nikitenko, "Tau Trigger Optimization in CMS Calorimeter," *Workshop on b/tau Physics at the LHC*, HIP, Helsinki 2002.
20. S. Lehti, R. Kinnunen, and J. Touominiemi, "Study of h, H, A → $\tau\tau$ → eμ in the CMS Detector," CMS Note 1998/019.
21. R. Kinnunen and A. Nikitenko, "Study of $H_{SUSY} \to \tau\tau \to \ell^{\pm} + \tau$ jet + E_t^{miss} in CMS," CMS Note 1997/106.
22. R. Kinnunen and D. Denegri, "The $H_{SUSY} \to h^{\pm} + h^{\mp} + X$ Channel, Its Advantages and Potential Instrumental Drawbacks," CMS Note 1999/037.
23. R. Kinnunen and A. Nikitenko, "Study of H → $\tau\tau$ With Hadronic τ Decays in CMS," CMS Note 2003/006.
24. P. Salmi *et al.*, "Prospects of Detecting Massive Charged Higgs from Hadronic Decay $H^{\pm} \to tb$ in CMS," CMS Note 2002/024.
25. R. Kinnunen, "Study for Heavy Charged Higgs in pp → $tH^{\pm}$ With $H^{\pm} \to \tau\nu$ in CMS," CMS Note 2000/045; R. Kinnunen, "Higgs Physics at LHC'," *SUSY02, The 10th International Conference on Supersymmetry and Unification of Fundamental Interactions*,CMS-CR-2002-020 (2002).
26. S. Abdullin *et al.*, "Search for SUSY at Large tanβ in CMS: The Low Luminosity Case," CMS Note 1999/018;

27. A. Tricomi, "Sparticle Searches with CMS at LHC," talk given at SUSY'02, Hamburg, CMS-CR-2002-022 (2002); M. Chiorboli, "Recent Studies on Sparticles and MSSM Higges at CMS," CMS-CR-2002-013 (2002); S. Villa, "Discovery Potential for SUGRA/SUSY at CMS," talk given at SUGRA20, Boston (2003).
28. J. Branson *et al.*, "High Transverse Momentum Physics at the Large Hadron Collider," *EPJdirect* **CN1** (2002) 1.
29. L. Randall and R. Sundrum, "A Large Mass Hierarchy from a Small Extra Dimension," *Phys. Rev. Lett.* **83** (1999) 3370.
30. P. Traczyk and G. Wrochna, "Search for Randall-Sundrum Graviton Excitations in the CMS Experiment," CMS Note 2002/003.
31. K. Abe *et al.*, "Search for New Gauge Bosons Decaying into Dielectrons in $\bar{\mathrm{p}}\mathrm{p}$ Collisions at $\sqrt{s} = 1.8$ TeV." *Phys Rev* **D51** (1995) 949.
32. M. J. G. Veltman, "Reflections on the Higgs System," CERN Academic Training Programme, 1996-1997.
33. E. Eichten, I. Hinchliffe, K. Lane, and C. Quigg, "Supercollider Physics", *Rev. Mod. Phys.* **56** (1984) 579.
34. "Physics Potential and Experimental Challenges of the LHC Luminosity Upgrade," F. Gianotti, M. L. Mangano and T. Virdee (Conveners), S. Abdullin *et al.* (Contributors), CERN-TH/2002-078 and hep-ph/0204087.
35. A. K. Gupta, S. Jain, and N. K. Mondal, "Search for Quark-Lepton Compositeness Using Dielectron Data at LHC," CMS Note 1999/075.
36. E. Rutherford, "The Scattering of α and β Particles by Matter and the Structure of the Atom," *Phil. Mag.* **21** (1911) 669.
37. J. D. Cockcroft and E. T. S. Walton, "Experiments with High Velocity Positive Ions. II The Disintigration of Elements by High Velocity Protons," *Proc. of the Royal Society, Series A*, **137** (1932) 229.
38. R. Hofstadter, H. R. Fechter, and J. A. McIntyre, "High Energy Electron Scattering and Nuclear Structure Determinations," *Phys. Rev.* **92** (1953) 978.
39. G. Arnison *et al.*, "Angular Distributions for High-Mass Jet Pairs and a Limit of the Energy Scale for Compositeness for Quarks from the CERN $\mathrm{p}\bar{\mathrm{p}}$ Collider," *Phys. Lett.* **177B** (1986) 244.
40. K. Hagiwara *et al.* (Particle Data Group), "Searches for Quark and Lepton Compositeness," *Phys. Rev.* **D66** (2002) 10001.
41. J. Rohlf, "Recent Results from the CERN $\mathrm{p}\bar{\mathrm{p}}$ Collider," *Proc. of the 12th International Conference on High-Energy Accelerators*, Fermilab (1983).
42. G. Arnison *et al.*, "Experimental Observation of Isolated Large Transverse Energy Electrons with Associated Missing Energy at $\sqrt{s} = 540$ GeV," *Phys. Lett.* **122B** (1983) 103; G. Arnison *et al.*, "Experimental Observation of Lepton Pairs of Invariant Mass Around 95 GeV/c^2 at the CERN SPS Collider," *Phys. Lett.* **126B** (1983) 398.
43. L. M. Lederman, "Introductory Greetings," *Proc. of the 12th International Conference on High-Energy Accelerators*, Fermilab (1983).
44. M. J. G. Veltman, private communication.
45. M. Della Negra, "Status of CMS," *Proceedings of the IV International Symposium on LHC Physics and Detectors*, Fermilab (2003).